Check for updates

Facile synthesis of mesoporous titanium dioxide doped by Ag-coated graphene with enhanced visible-light photocatalytic performance for methylene blue degradation†

Lin Xiao, Li Youji, [iD]* Chen Feitai, Xu Peng and Li Ming

A highly efficient and elaborately structured visible-light-driven catalyst composed of mesoporous TiO_2 (MT) doped with Ag^+-coated graphene (MT-Ag/GR) has been successfully fabricated by a sol–gel and solvothermal method. The as-prepared catalyst has been investigated by X-ray diffraction (XRD), photoluminescence spectroscopy (PL), X-ray photoelectron spectroscopy (XPS), diffuse reflectance spectroscopy (DRS), scanning electron microscopy (SEM), Fourier transform infrared (FT-IR) spectroscopy, and transmission electron microscopy (TEM). Inexpensive, stable MT was coupled with hole-accepting graphene (GR) and electron-trapping silver induced higher activities than those achieved with pure MT, MT-Ag, and MT/GR in the degradation of methylene blue (MB) in solution. Although the Ag dopant and graphene support were responsible for narrowing the band gap of TiO_2 and shifting its optical response, respectively, they acted synergistically in shifting absorbance from the ultraviolet (UV) to the visible-light region with a smaller band-gap energy. Meanwhile, they also served to lower the photo-induced electron and hole recombination rate, and increased the specific surface area and the concentrations of Ti^{3+} ions and hydroxyl groups. In degradation studies, the effects of catalyst amount, pH, and initial MB concentration have been examined as operational parameters. A photocatalytic mechanism for the action of MT-Ag/GR is proposed, and possible reasons for the enhancement in visible-light photocatalytic efficiency are discussed.

1. Introduction

Mesoporous TiO_2 (MT) has been demonstrated to be a highly effective photocatalyst because of its large surface area, porous structure, and large pore volume, which result in an increased number of surface reactive sites and improved mass transport, and it is also environmentally friendly.[1–3] Nevertheless, there are still restrictions for its application, such as a high recombination rate of photo-generated electrons and holes, and a low photoresponse towards visible light. These two limiting factors make MT a less-than-ideal material for effective photocatalysis. Therefore, various efforts have been made to improve the photocatalytic properties of MT, including doping with metal ions and coupling with a second semiconductor.[4–6] To enhance the visible-light-driven photocatalytic performance of MT, noble metals (Pt, Ag, Pd, Au) have been widely used as dopants to extend its light absorption into the visible-light region.[7–11] Ag is frequently employed in surface-modified semiconductor heterojunctions due to its Schottky barriers and matched energy levels.[8,9] However, the modified MT also incurs some loss of photocatalytic activity due to an inherent decrease in the surface area available for reaction and low electrical conductivity of the heterostructure.[12] Thus, there is a need to develop a reliable approach to synthesize highly efficient visible-light-driven MT with a tailored structure. Several studies are currently focused on the synthesis of MT on graphene (GR) sheets due to the unique properties, such as excellent electron rich entity, large surface area, and unrivalled electrical conduction.[12–14] Under UV or visible-light irradiation, the photocurrent generation of GR–TiO_2 is superior to that of TiO_2 because GR with the π–π conjugated structure of the carbon atoms can help in dispersion of e^- or h^+ reducing charge recombination.[15–17] Thus, the addition of GR to bulk TiO_2 has been observed to improve activity under visible-light irradiation for the degradation of dodecyl benzenesulfonate,[18] methylene blue (MB),[19] Eosin blue dye,[20] and texbrite pollutants.[21] However, little effort has seemingly been made to combine Ag, GR, and MT. Herein, a visible-light-driven MT catalyst is proposed, considering the synergistic effects of the GR support and Ag doping on the structure and photocatalytic activity of MT. A sol–gel and solvothermal method with the aid of a liquid-

College of Chemistry and Chemical Engineering, Jishou University, 416000, Hunan, P. R. China. E-mail: bcclyj@163.com; Tel: +86-13762157748

crystal template has been applied to fabricate MT modified by Ag together with graphene (MT-Ag/GR), thereby generating a catalyst with elaborate structure and high photoactivity. A photocatalytic mechanism for MB degradation by visible-light based MT-Ag/GR is proposed and possible reasons for the enhancement of visible-light photocatalytic efficiency are discussed. Additionally, to optimize the catalytic performance of MT-Ag/GR, the effects of catalyst amount, pH, and initial MB concentration have been examined as operational parameters.

2. Experimental

2.1. Materials

Graphene oxide (GO) was purchased from Changsha FENHUA Materials Technology Corporation Limited, Changsha, People's Republic of China. Cetyl trimethylammonium bromide (CTAB, 99 wt%), and butyl titanate were purchased from Tianjin Guangfu Fine Chemical Research Institute. Absolute ethanol, silver nitrate, and concentrated nitric acid were purchased from Hunan Huihong Reagent Corporation Limited. All reagents were used as received without further purification.

2.2. Fabrication of MT-Ag/GR

Firstly, cetyl trimethylammonium bromide (CTAB, 5.0 g) was mixed with ethanol (30 mL) and stirred steadily to form a liquid-crystal template (LCT) at ambient temperature. Subsequently, a solution of butyl titanate (25 mL) in absolute ethanol (50 mL) was slowly added to the LCT at a rate of one drop every 3 s and stirred for a certain time to form a titanium dioxide sol containing the LCT. Next, a solution of 7.0 mg AgNO$_3$ in 5.0 mL ethanol and the 10 mL graphene oxide solution in ethanol (2.0 mg mL^{-1}) were mixed and then slowly added to the titanium dioxide sol/LCT. Throughout the whole process, the solution was stirred until it formed a titanium dioxide gel. Subsequently, the obtained gel was dried at 65 °C and then calcined at 450 °C under the protection of nitrogen to prepare an MT-Ag/GR nanocomposite. Following a similar protocol, but without silver nitrate or GO, mesoporous titania combined with graphene (MT/GR) and Ag-doped mesoporous titania (MT-Ag) were synthesized.

2.3. Characterization of the material

The crystalline phase of the obtained samples was identified by means of a Y-2000 X-ray diffractometer (Bruker, Germany) using Cu-K$_\alpha$ radiation from an 18 kV source. Low-angle XRD patterns were acquired on a Nano STAR X-ray diffractometer using Cu-K$_\alpha$ radiation from a 40 kV source. The Brunauer–Emmett–Teller (BET) specific surface area and pore size distribution of samples were measured from N$_2$ adsorption/desorption isotherms determined at liquid-nitrogen temperature (77.3 K) on a Quantachrome Instruments Autosorb-1-C/TCD. PL spectra of the samples were acquired on a Varian Cary Eclipse spectrometer. The surface morphology and size of products was characterized by N3400 scanning electron microscopy (SEM) and JEM-2010F transmission electron microscopy (TEM). UV/Vis diffuse-reflectance spectra were recorded at room temperature on a Lambda 20 spectrophotometer (Perkin-Elmer, USA). Fourier

transform infrared (FT-IR) spectrum was recorded on a Nicolet Is10 fourier red spectrometer (Nicolet, America). X-ray photo-electron spectroscopy (XPS) was performed on an instrument from Kratos Analytical Ltd. (England).

2.4. Photocatalytic evaluation

The photocatalytic reactor used has been described previously.[22] The visible radiation source is a high-pressure Hg lamp with UV filter; the highest intensity of this lamp is in the region 450–900 nm. The suspension was placed in the reactor, and air was bubbled through it at a rate of 10.0 mL s^{-1} in order to maintain a homogeneous mixture. To establish an adsorption–desorption equilibrium, the suspension was continuously stirred for 30 min in the dark prior to irradiation. At given irradiation time intervals, 3 mL of the suspension was collected and subsequently centrifuged to remove the catalyst particles. The concentration was determined by measuring the maximum absorbance of MB at 664 nm with a TU-1810 spectrophotometer. To compare reaction rates among different catalysts, a pseudo-first-order rate equation was introduced as follows:

$$-\frac{\mathrm{d}C}{t} = k_{\mathrm{app}}C \tag{1}$$

where C is the MB concentration at time t and k_{app} is the apparent reaction rate constant. This equation can be integrated to give the following form:

$$\ln \frac{C_0}{C} = k_{\mathrm{app}}t \tag{2}$$

where C_0 is the initial concentration of MB and C is the concentration of MB after t minutes of visible irradiation. According to Beer's law, the absorbance at 664 nm (the characteristic absorption wavelength of MB) is proportional to the concentration of MB in the reaction solution, so $\ln(C_0/C)$ equates to $\ln(A_0/A)$, where A_0 is the solution absorbance at time zero and A is the solution absorbance at time t after turning on the lamp.

3. Results and discussion

3.1. Characterization of catalysts

3.1.1. XRD analysis. As shown in Fig. 1a, all samples exhibited a diffraction peak at around $2\theta = 0.5°$, corresponding to the (100) reflection of MT. This indicated that all samples maintained a highly ordered mesostructure, and that
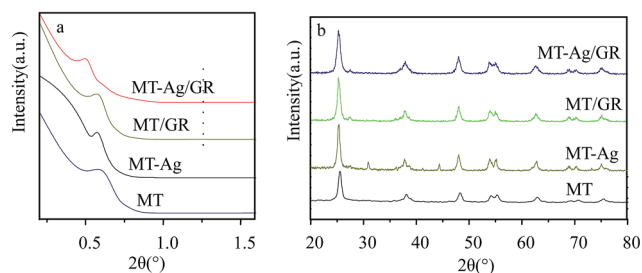

Fig. 1 Effects of low angle (a) and XRD (b) patterns of samples.

modification with Ag and GR did not disrupt the mesoporous structure of pure MT. However, the intensity of the characteristic diffraction peak for the nanocomposites was smaller than that for pure MT, and it was also shifted to a smaller angle. This implied that modification by the Ag dopant or GR support decreased the pore size of MT. However, MT-Ag/GR retained a strong characteristic diffraction peak, showing that the modifications with Ag and GR did not lead to collapse of the mesopores of MT. As shown in Fig. 1b, the diffraction peaks at 25.2°, 26.1°, 37.66°, 48.0°, 54.26°, 55.02°, and 62.74° can be readily indexed to the (101), (110), (004), (200), (105), (211), and (214) planes of anatase and rutile TiO_2, respectively (JCPDS no. 21-1272). It can also be seen from Fig. 1b that for the MT-Ag sample, after loading Ag on TiO_2, the 2θ positions of the major diffraction peaks have similar values to those of pristine TiO_2, except for an additional peak at $2\theta = 45.2°$, which can be attributed to the (200) crystalline plane of metallic Ag. For MT-Ag/GR, the characteristic peaks of TiO_2 could again be seen, without any change in 2θ position, but the peak assigned to Ag metal at 31.5° and 45.2° in the XRD pattern of the MT-Ag sample could no longer be seen. This was consistent with oxidation of Ag to Ag_2O by GR in the nanocomposite structure during the sol–gel and solvothermal process. The characteristic peak of Ag_2O appears at $2\theta = 38°$, which in the case of MT-Ag/GR overlaps with the peaks of TiO_2. For this reason, no peak could be discerned for this compound, but other characterization methods, such as XPS and TEM (see below) demonstrated its presence.[23,24] Notably, no characteristic diffraction peaks attributable to discrete graphene sheets were observed in the nanocomposite diffraction patterns of MT/GR or MT-Ag/GR. This may have been because the main characteristic peak of graphene at 24.5° was obscured by the main peak of anatase TiO_2 at 25.4°.[23] Besides, the presence of Ag and GR may have broadened the [101] peak of anatase and decreased the MT crystallite size by hindering crystal growth. Additionally, in contrast to other carbon materials, which hinder crystal transformation,[25] GR can promote the crystal transformation of MT due to its high-temperature thermal effect.[26]

3.1.2. UV/Vis diffuse-reflectance spectroscopy. The optical properties of the various photocatalysts are shown in Fig. 2. As expected, the main absorption edge of MT was estimated to be about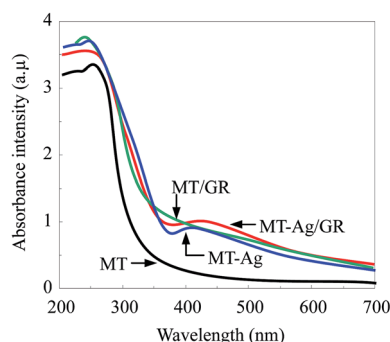 387 nm (3.2 eV) due to the intrinsic band-gap absorption of TiO_2.[27] The onsets of the absorption spectra of MT-Ag, MT/GR, and MT-Ag/GR were shifted to the visible region due to the Ag dopant, GR support, or their synergistic effect. From the UV/Vis spectra of these samples, the energy band-gap values can be estimated by using the Kabelka–Munk function were 2.95, 2.82, and 2.73 eV for MT-Ag, MT/GR, and MT-Ag/GR, respectively. Evidently, MT-Ag/GR showed the smallest band-gap energy in the visible-light range mainly due to the synergistic effect of Ag and GR on MT. The peak at 410 nm corresponds to the characteristic absorption of Ag in the MT-Ag nanostructure with Schottky barrier. Meanwhile, GR sheets have easily excitable electrons for transfer to CB of MT resulting reduced band gape of composite materials, effectively extending the absorption into the visible-light region.[18,19,23,24]

3.1.3. Photoluminescence spectra and electron/hole recombination. Photoluminescence (PL) spectra provide insight since the PL intensity gives a direct measure of the electron–hole recombination rate, that is, the faster the recombination, the more intense the spectral peak. Based on the PL characteristics of MT, a lower intensity indicates that more excited electrons are trapped and stably transferred through the interface.[28] As shown in Fig. 3, the interactions among TiO_2, GR, and Ag could be monitored by measuring the PL decay of the samples. The PL intensities gradually increased in the order MT-Ag/GR < MT/GR < MT-Ag < MT, such that the MT-Ag/GR sample had the lowest intensity. This was presumably due to the following reasons: (1) due to their two-dimensional π-conjugated structure with the easily excitable electrons, so GR can disperse h^+, reducing the recombination rate of electron–hole pairs and thereby decreasing the PL signal intensity; (2) the interface between Ag and MT constituted a Schottky junction, resulting in a separation of photoelectrons and holes by trapping the electrons. These results suggested that the formation of the MT-Ag/GR nanostructure decreased the recombination of photogenerated electrons and holes and improved the photocatalytic ability of the MT-Ag/GR nanostructure. This was further confirmed by photocatalytic experiments.

3.1.4. SEM and TEM analysis. SEM micrographs were used to observe the morphology of the as-prepared photocatalysts as

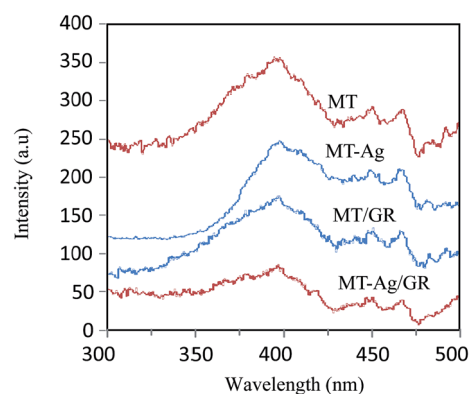**Fig. 2** UV-vis diffuse reflection spectra of samples.

Fig. 3 Room temperature PL emission spectra of different photocatalysts excited at a wavelength of 260 nm.

shown in Fig. 4. The MT obviously show spherical shape consisted of nanoparticles with some pores (Fig. 4a). Comparison of the SEM micrograph of pure MT-Ag and MT nanoparticles proved that doping of Ag nanoparticles did not affect the spherical shape of MT nanoparticles (Fig. 4b). And smooth surface sheet structure of the GR can be clearly observed in the SEM images (Fig. 4c). The morphology of the MT-Ag/GR is porous, sponge-like shape and wrinkled edges, and there are also many pores in its structure which increase the surface area (Fig. 4d). The surface modification and particle sizes of the samples were investigated by TEM. The two-dimensional structure of GR sheets is shown in Fig. 5a, which clearly reveals μm-scale wrinkles. As shown in Fig. 5b, the pure MT particles did not disperse well, leading to inconspicuous mesopores, and only a few clusters could be explicitly identified. And from seen magnified image inserted in Fig. 5b, the particle size of MT was less than 50 nm, with spherical morphology. It is evident from Fig. 5c that the particle size of MT-Ag was about 40 nm, smaller than that of pure MT, due to the hindering effect of Ag on the crystal growth of MT. TEM permitted easy differentiation of Ag nanocrystals on the surface of the MT particles as small dots in the size range 5–10 nm, which were incorporated at interstitial positions of the semiconductor particles. Additionally, a great enhancement of the homogeneity of pure MT could be realized by the GR support (Fig. 5d), with small particles of 40 nm due to its hindering effect on the agglomeration of MT particles. Similarly, MT-Ag particles were uniformly distributed on the surface of GR without obvious agglomeration, and the mesoporous structure was clearly seen for the MT-Ag/GR nanocomposite (Fig. 5e). Additionally, comparison of the TEM images of the prepared nanocomposites with those of the other samples confirmed that MT-Ag/GR had the smallest particle size due to the hindering effects of GR and Ag on the

growth of MT particles.[29] Thus, the facile synthesis of MT-Ag/GR, with its superior structure, offers a promising route for the rational design of comparatively inexpensive and highly active MT-based ternary nanostructured composites. The microstructure of the composite was further investigated by HRTEM (Fig. 5f). Crystal lattices of about 0.351, 0.338, and 0.231 nm could clearly be discerned, representative of anatase (101), graphene (002), and Ag (111) planes, respectively. The results corroborated that graphene had been successfully supported on MT, with concomitant doping by Ag.

3.1.5. FT-IR spectra of samples. As shown in Fig. 6, the FT-IR spectra of samples show a strong and broad peak at 3400 cm^{-1}, indicating the presence of a surface O–H stretching vibration besides MT,[27] suggesting more hydroxyl in GR-supported samples. Additionally, GR exhibits two peaks at 1630 and 1350 cm^{-1} for C=O and C=C groups, respectively. The GR still contains some oxygen containing functionalities, which can induce interactions of GR with titania and Ag nanoparticles. Peaks at 2854 and 2927 cm^{-1} imply the presence of CH$_2$ groups in GR. Notably, the intensity of CH$_2$ decreases in GR-supported samples, which proves the successful interaction of GR to MT or Ag. The band in the range of 400–1000 cm^{-1} corresponds to the Ti–O stretching vibration of crystalline TiO$_2$ phase,[23] suggesting the existence of both Ti–O–Ti and Ti–O–C bonds in the composites. Moreover, the 400–1000 cm^{-1} line shape of MT-Ag/GR is the same as that of MT/GR, and different from that of Ag/GR. It obviously reveals the linkages between GR with MT in MT-Ag/GR mainly due to the low amount of the doped Ag.

3.1.6. N$_2$ adsorption/desorption isotherm analysis. As can be seen from Fig. 6a, the isotherms of all the samples were of the typical Langmuir type IV form, suggesting that mesopores were widely distributed therein.[29,30] Compared to the isotherm
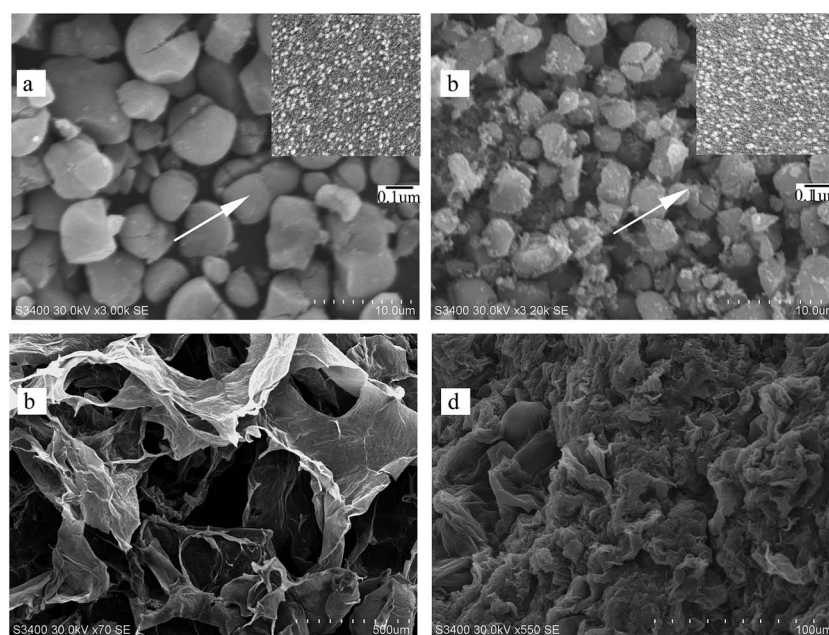

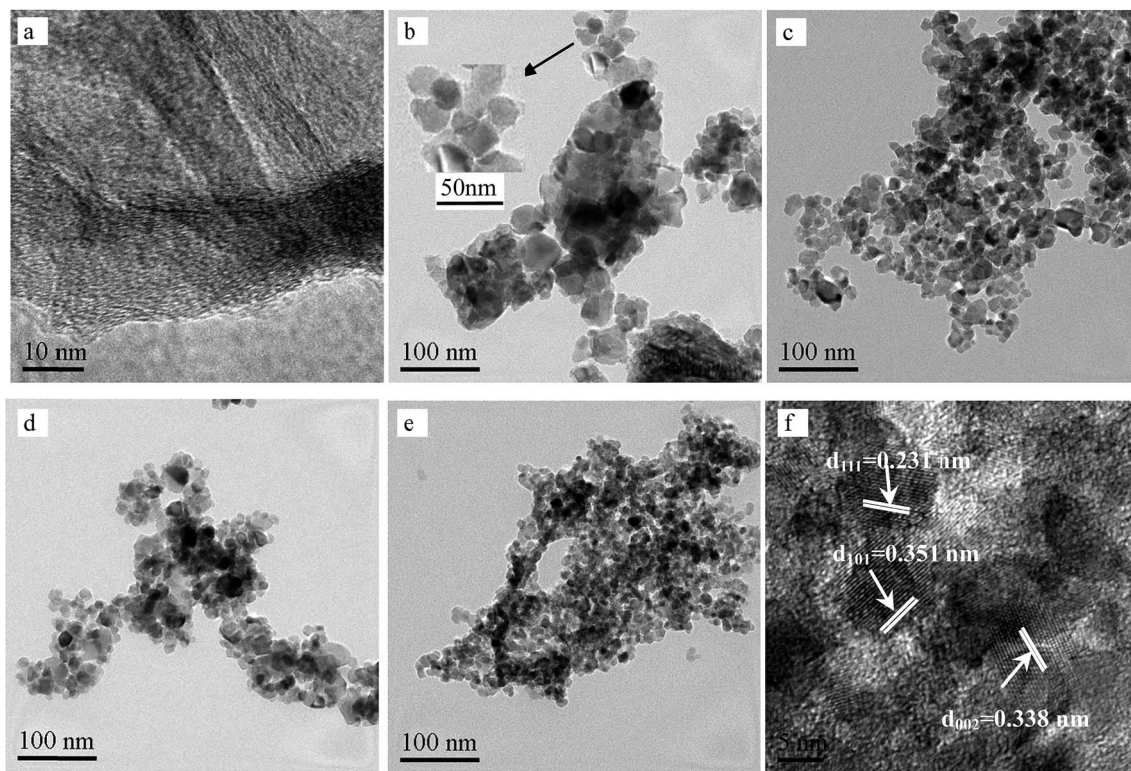**Fig. 4** SEM of samples ((a) MT; (b) MT-Ag; (c) GR; (d) MT-Ag/GR).

Fig. 5 TEM of samples ((a) GR (b) MT; (c) MT-Ag; (d) MT/GR; (e) MT-Ag/GR with its HRTEM (f)).

of MT-Ag, with a typical H3 hysteresis loop, the isotherms of the other samples presented H2 hysteresis loops. Meanwhile, the hysteresis loop of MT/GR was also obviously different from those of pure MT and MT-Ag/GR. This indicated that the mesoporous structure of MT was changed by Ag or GR modification, consistent with the shapes of the pore size distribution curves (Fig. 7b). All pore sizes of the samples were in the range 9–50 nm, indicating the presence of mesopores with a slit-shaped structure. By incorporating Ag or GR, the surface area and pore volume of MT were increased and its pore size decreased, as determined by N_2 physisorption experiments as listed in Table 1. MT-Ag/GR showed the highest surface area and pore volume, but the lowest pore size. The porosity difference may be attributed either to the stacking structure or the introduction of GR and Ag, prevented the agglomeration of MT particles.[23]
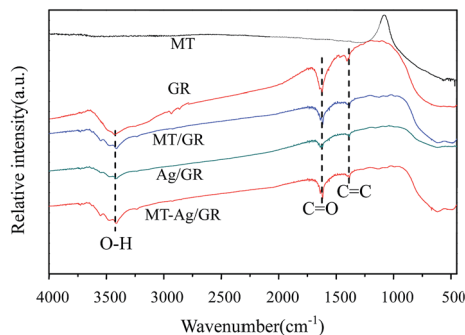
3.1.7. XPS analysis. The surface composition and chemical state of the products were further investigated by X-ray photoelectron spectroscopy. Fig. 8a shows the XPS survey spectrum of TM-Ag/GR, demonstrating that it contained Ag, Ti, O, and C. XPS Ti 2p spectra of the nanocomposites (Fig. 8b) showed Ti $2p_{3/2}$ and Ti $2p_{1/2}$ spin-orbital splitting photoelectron peaks located at binding energies of 459.2 and 464.9 eV, respectively, slightly shifted toward higher values compared with those of pure MT (458.5 and 464.2 eV). This result is consistent with previous reports.[10,30] It also implies that Ti in the nanocomposites was in an environment different from that of pure anatase, and that strong interaction between MT layers and Ag or GR modified the integrity of the TiO_2 structure. This property is beneficial to the photocatalysis because Ti with high binding energy in nanocomposites can be easily reduced to produce high content of Ti^{3+} ion (Table 1). As an active center, Ti^{3+} can
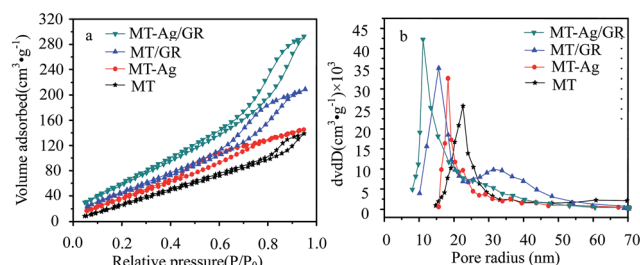

Fig. 6 FI-IR spectra of samples.

Fig. 7 N_2 adsorption–desorption isotherms (a) and pore size distributions (b) of the samples.

Table 1 Specific surface areas, total pore volumes, and pore sizes of pure MT, MT-Ag, MT/GR, and MT-Ag/GR

Samples	S_{BET} (m^2 g^{-1})	V_t (cm^3 g^{-1})	Pore radius (nm)	$\cdot$OH concentration (%)	Ti^{3+} concentration (%)
MT	129.729	0.206	22.620	11.7	4.6
MT-Ag	169.321	0.211	18.303	13.6	9.7
MT/GR	194.540	0.306	15.597	14.9	11.3
MT-Ag/GR	242.272	0.425	11.099	16.5	14.5
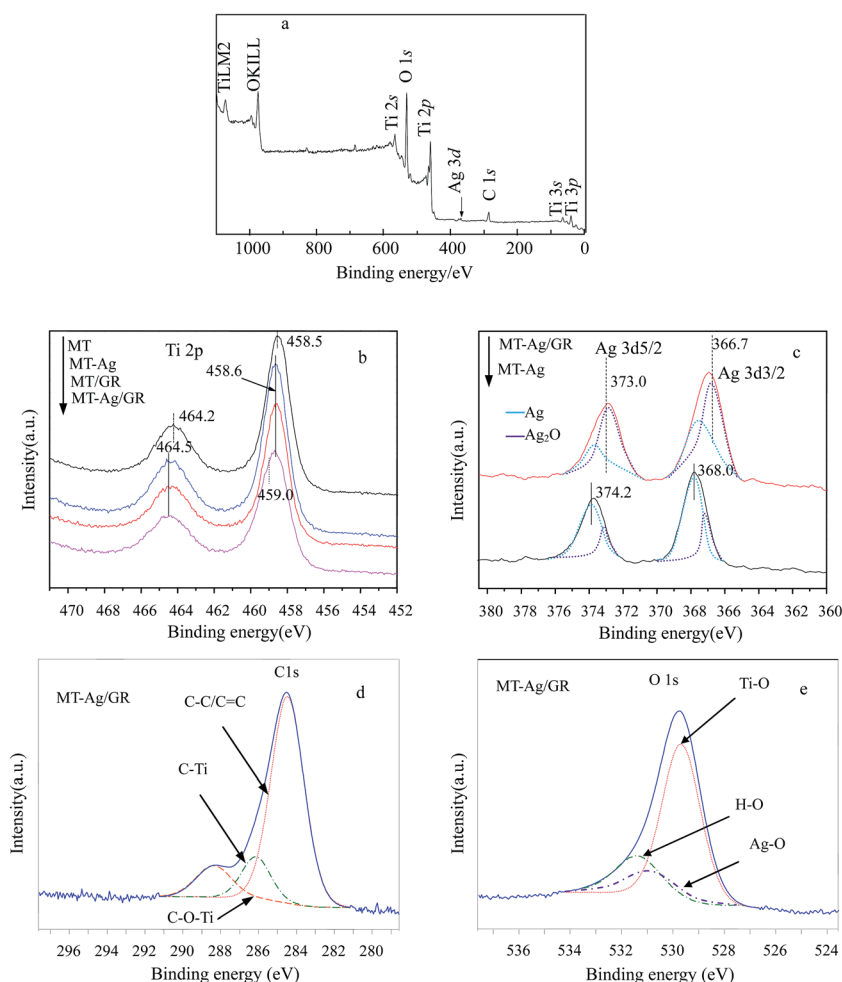
Fig. 8 Survey XPS spectrum of TM–Ag/GR (a), split peak fitting patterns of Ti 2p (a), Ag 3d (b), C ls (c) and O 1s (d) of the different photocatalysts.

trap photogenerated electrons in the conduction band and prevent the recombination of electron–hole pairs.[11] As shown in Fig. 8c, each Ag-containing sample showed two peaks attributable to metallic Ag centered at about 368.0 and 374.2 eV corresponding to Ag 3d$_{5/2}$ and Ag 3d$_{3/2}$ transitions, respectively, whereas peaks related to Ag$_2$O were centered at about 366.7 and 373.0 eV. The binding energies of Ag in MT-Ag have been mainly determined as 367.7 and 374.0 eV for Ag 3d$_{5/2}$ and Ag 3d$_{3/2}$, respectively, indicating the presence of many Ag metal.[31] Although main peaks at 366.7 and 373.0 eV for Ag 3d$_{5/2}$ and Ag 3d$_{3/2}$ in MT-Ag/GR have been attributed to the presence of many Ag$_2$O, MT-Ag/GR still has metallic silver.[23] These results are in accordance with the XRD analysis in Fig. 1. Additionally, the Ag

3d core-level XPS spectrum of MT-Ag/GR indicated a decrease in binding energy by about 0.8 eV compared to the Ag 3d binding energy for the MT-Ag sample, consistent with the oxidation of Ag^0 to Ag$^+$ and the formation of Ag$_2$O.[32,33] The C 1s XPS signals of MT-Ag/GR are shown in Fig. 8d. There are mainly three forms of C-bonds present in the samples, namely C–Ti, C–O–Ti, and C–C or C=C. The largest binding energy of about 284.8 eV is representative of C–C or C=C bonds in graphene. Peaks at higher binding energies can be assigned to oxygenated carbon species, such as C–O.[34] Note that the content of oxygen functional groups significantly decreased after reduction during the sol–gel process. However, some of these oxygen functional groups remained after reduction of GO because MT/GO was not

completely reduced to graphene. The presence of C–Ti bonds can be assigned to the combination of carbon and MT, and the intensity of the C–Ti signal of MT-Ag/GR was obviously stronger than that of MT, further demonstrating that GR was well supported on MT. The presence of Ti–O–C carbonaceous bonds at the sample interface has been attributed to coordination between carboxyl groups of GR and Ti(OH)$_x$.[35] The XPS O 1s signals corresponded to Ti–O at 529.8 eV and H–O at 531.5 eV (Fig. 8e). That at 529.8 eV was due to O^{2-} ion in the TiO$_2$ lattice, whereas the shoulder peak located at a binding energy of 531.5 eV can be attributed to the surface hydroxyl groups of chemisorbed water molecules on the titania.[34,36] The hydroxyl concentration increased for these samples in the order: MT < MT-Ag < MT/GR < MT-Ag/GR, mainly due to their different surface areas (Table 1). The H–O concentration of MT-Ag/GR was apparently higher than those of the other photocatalysts, as a result of its large specific surface area, which can provide more space to store ·OH radicals, thereby leading to higher photocatalytic activity.

3.2. Photocatalysis

3.2.1.   Photocatalytic performance and mechanism of MT-Ag/GR in MB degradation process. Before carrying out the photocatalytic degradation of MB, it was established that the absorption rate of the catalysts was in the range 3–7% without illumination (Fig. S1†), which would have little effect on the photocatalytic degradation and could thus be ignored in comparison. As shown in Fig. 8, the photocatalytic performances of commercial P25, as-prepared MT, MT-Ag, MT/GR and MT-Ag/GR nanocomposite were assessed by deploying them in the degradation of MB as a model reaction under visible light and UV light irradiation. Fig. 9a shows the normalized concentration against the time for different reaction mixtures. Under the non-catalyst (only MB) conditions, the degradation of MB after 60 min of visible light exposure is negligible. This indicates that MB neither self-degrades under visible light exposure. In comparison with commercial P25 (36.7%), pure MT exhibited a better photocatalytic performance (Fig. 9a), with a degradation rate of 53.4% under UV irradiation for 160 min, due to its higher surface area. Furthermore, the photocatalytic performances of the nanocomposites MT-Ag, MT/GR, and MT-Ag/GR under visible light were superior to that of MT under UV irradiation owning to the high

concentrations of Ti^{3+} ions and hydroxyl groups besides small band-gap energy. MT/GR showed high visible-light catalytic performance, with a degradation rate of 72.5%, because GR with a two-dimensional π-conjugated structure is electron rich entity may accept h$^+$ and suppress charge recombination. MT-Ag also showed an MB degradation rate of 81.7% under visible light illumination due to the formation of a Schottky barrier, at which Ag can serve as an electron trap, preventing electron–hole recombination.[37] Moreover, MT-Ag/GR show the highest photocatalytic performance with almost complete degradation of MB solution for the same time. The kinetics of the photocatalytic degradation of MB has been discussed in terms of the Langmuir–Hinshelwood mechanism.[14,19] As can be seen from Fig. 9b, the rate constants with P25, MT, MT-Ag, MT/GR, and MT-Ag/GR were 0.0033, 0.0049, 0.0063, 0.0081, and 0.0119 h^{-1}, respectively. The obtained degradation rate on MT-Ag/GR was thus 3.6, 2.4, 1.9, and 1.4 times greater than those on P25, MT, MT-Ag, and MT/GR, respectively. MT-Ag/GR showed the highest photocatalytic performance among all of the studied catalysts. This result is closely related to the combined effects of Ag doping and the GR support in improving the separation of photogenerated electron–hole pairs. Therefore, the cooperation of Ag, GR, and MT can greatly improve the photocatalytic efficiency, such that it may even be stimulated by visible light. Additionally, with each reuse, the photocatalytic activity of MT-Ag/GR slightly decreased, but the rate constant remained almost stable at 0.0075 min^{-1} after the third recycling. This suggests that the MT-Ag/GR maintains high photocatalytic activity after recycling. MT-Ag/GR maintains high photocatalytic activity in cyclic usage mainly because of the almost negligible detachment of MT-Ag from GR after repeated use (Fig. 10). On the basis of the above experimental results and discussion, we surmise that the improved photocatalytic performance arises from the enhanced light harvesting and more efficient separation of photogenerated electron–hole pairs with the MT-Ag/GR nanocomposite. A possible mechanism for the photocatalytic degradation of MB by MT-Ag/GR can thus be proposed, and a schematic diagram illustrating the behavior of the radicals is shown in Fig. 11. The relevant reactions are expressed by eqn (3)–(10). MT in MT-Ag/GR contains a lot of defects, particularly due to heterojunctions that decrease the energy of its conduction band as much as 1 eV.[38] Therefore, it is possible that such types of titania can absorb visible light to
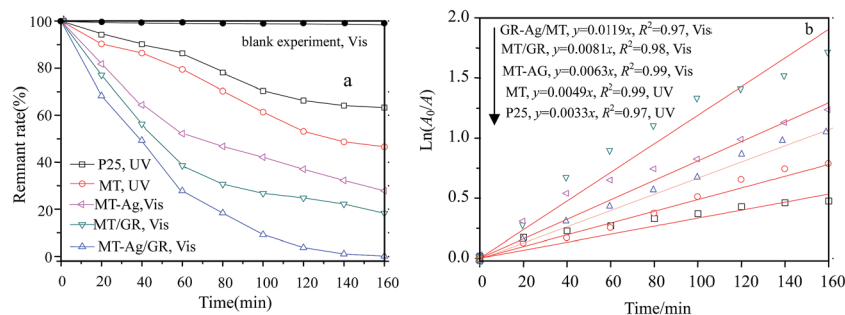

Fig. 9 Relationships between catalytic time on MB degradation rate (a) and ln(A_0/A) (b).
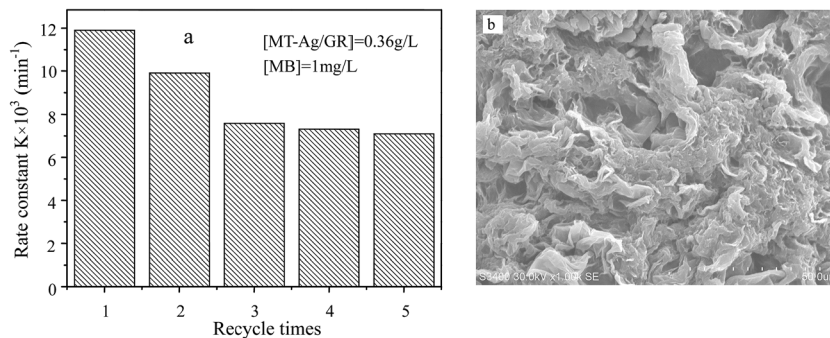
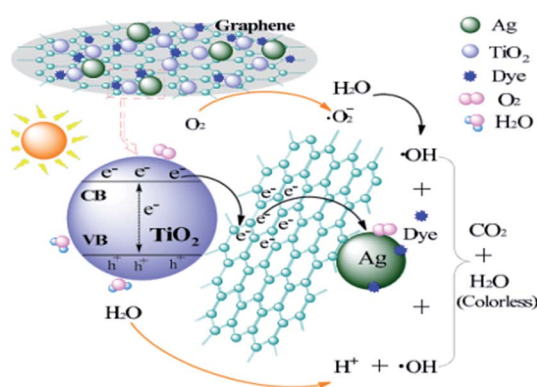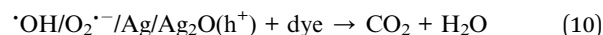Fig. 10 Recycling performance of MT-Ag/GR for MB degradation (a) and SEM image of used MT-Ag/GR (b).
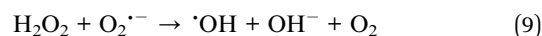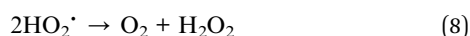

Fig. 11 Mechanism of the photocatalytic process using MT-Ag/GR under visible light.

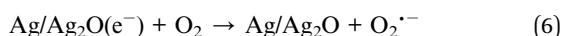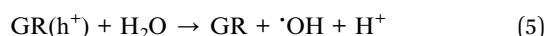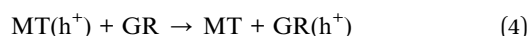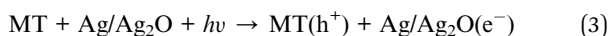promote electrons from the valence band to the conduction band. These electrons can then be transferred to the Ag clusters that are deposited on MT (eqn (3)). The photogenerated holes from MT (h^+) can be captured by the GR sheet and then react with H_2O to afford ·OH radicals and H^+ (eqn (4) and (5)). Additionally, the residual electrons ($Ag(e^-)$) can utilized for the reduction of oxygen, thus forming $O_2^{·-}$ radical species (eqn (6)). The H^+ and superoxide radical anion $O_2^{·-}$ can then be further transformed to ·OH radicals by a series of reactions (eqn (7)–(9)). Subsequently, the $O_2^{·-}$ and ·OH radicals, together with the photogenerated holes in the Ag nanocrystals, can directly oxidize the organic dye (eqn (10)) to colorless small molecules (H_2O and CO_2), accomplishing complete destruction of the organic molecules along with color removal (Fig. S2†).[14,19,21]

$$MT + Ag/Ag_2O + hv \rightarrow MT(h^+) + Ag/Ag_2O(e^-) \tag{3}$$

$$MT(h^+) + GR \rightarrow MT + GR(h^+) \tag{4}$$

$$GR(h^+) + H_2O \rightarrow GR + ·OH + H^+ \tag{5}$$

$$Ag/Ag_2O(e^-) + O_2 \rightarrow Ag/Ag_2O + O_2^{·-} \tag{6}$$

$$O_2^{·-} + H^+ \rightarrow HO_2^· \tag{7}$$

$$2HO_2^· \rightarrow O_2 + H_2O_2 \tag{8}$$

$$H_2O_2 + O_2^{·-} \rightarrow ·OH + OH^- + O_2 \tag{9}$$

$$·OH/O_2^{·-}/Ag/Ag_2O(h^+) + dye \rightarrow CO_2 + H_2O \tag{10}$$
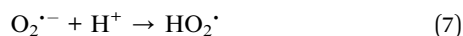
3.2.2. Effects of reaction conditions on photocatalytic activity. Fig. 12 depicts the main influencing factors on photocatalytic activity, including the initial concentration of MB, pH, and the catalyst loading. The photocatalytic activity of MT-Ag/GR sharply decreased when the initial concentration of MB was increased from 1 mg L^{-1} to 5 mg L^{-1}, and higher MB concentrations led to lower photocatalytic activity (Fig. 12a). This can be explained as follows. For a certain amount of MT-Ag/GR, the number of active centers thereon is finite, and so the photodegradation rate decreases with increasing initial concentration of MB, possibly because of a concomitant decrease in solution permeability and a reduction in visible light absorption by the catalyst under constant irradiation. Thus, the photocatalytic activity is diminished at high MB concentrations. The pH is also an important factor in influencing the photocatalytic process. It was clearly observed that pH 6 was advantageous for the photocatalytic reaction of MB (Fig. 12b). Strongly acidic or alkaline conditions were not conducive to the decomposition of MB. This can be explained by the fact that under relatively strongly acidic conditions (pH < 6), the surface of the catalyst would be occupied by H^+, making ·OH radicals difficult to generate. In a weakly acidic photocatalytic system (pH 6), positive charges accumulate on the surface of TiO_2, and ionic interactions between cationic dye molecules and negatively charged groups can be formed in the vicinity of abundant π–π conjugations between MB molecules and the aromatic rings of the graphene sheets,[38] thereby facilitating the photocatalytic activity. When the pH is further increased beyond 6, fewer H^+ is dispersed on the surface of the catalyst, resulting in less adsorption of MB and hence reduced photocatalytic degradation. Consequently, low and high pH values are not conducive to MB adsorption and hydroxy group production on MT-Ag/GR, respectively. The optimum pH for the photocatalytic degradation process of MB is that at which there is a high concentration of hydroxy groups and plentiful MB on MT-Ag/GR. The reaction rate as a function of catalyst concentration is important.[14] Hence, a series of experiments was carried out to find the optimum catalyst concentration by
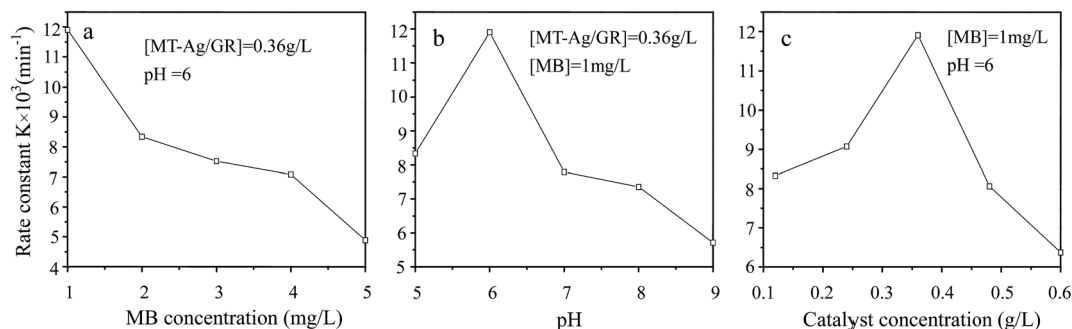
Fig. 12 Relative curves of degradation rate constant K by MB initial concentration (a), pH (b) and catalyst concentration (c).

varying this parameter from 0.1 to 0.6 g L^{-1} (Fig. 12c). Turbidity of the solution above 0.36 g L^{-1} reduced light transmission through it, whereas below this level adsorption on the MT-Ag/GR surface and the absorption of light were the limiting factors. It is reported that the catalyst concentration has both positive and negative impacts on the photodecomposition rate. An increased concentration of the catalyst increases the quantity of photons absorbed and consequently the degradation rate. However, a further increase in catalyst concentration beyond 0.36 g L^{-1} may result in deactivation of the activated molecules due to collision with ground-state molecules.[39,40] At concentrations higher than 0.36 g L^{-1}, MT-Ag/GR aggregation (particle–particle interactions) may commence and lower the effective surface area of the catalyst, thereby suppressing adsorption of the reactant.

4. Conclusions

In this study, an MT-Ag/GR nanocomposite showing superior catalytic performance has been synthesized by a facile sol–gel and solvothermal method with the aid of a liquid-crystal template. It was noted that the incorporation of graphene and Ag can effectively improve the photocatalytic activity of TiO$_2$ by increasing its adsorption property, inhibiting charge recombination, and reducing the band-gap energy. The MT-Ag/GR hybrid exhibited superior photocatalytic activity in the degradation of MB dye compared with bare MT, P25, MT-Ag, and MT/GR. Furthermore, the degradation capacity of MT-Ag/GR did not display any discernible decrease after four degradation cycles. The superior properties of the nanostructure could be related to the presence of graphene sheets with hole-accepting property and metallic silver with electron-trapping property, which decreases the photo-induced electron–hole recombination rate and broadens the light response range. A plausible mechanism for the degradation of MB by photocatalytic oxidation under visible light on MT-Ag/GR has been proposed. Additionally, the optimal conditions were identified as an MB concentration of 1 mg L^{-1} at pH 6 with an MT-Ag/GR concentration of 0.36 mg L^{-1}. The dual incorporation of graphene with a unique porous structure and noble metals into semiconductor structures offers a promising strategy for fabricating highly active ternary nanostructured nanocomposites for water purification under solar irradiation.

References

1 J. G. Yu, Y. R. Su and B. Cheng, Template-Free Fabrication and Enhanced Photocatalytic Activity of Hierarchical Macro-/Mesoporous Titania, *Adv. Funct. Mater.*, 2007, **17**, 1984–1990.

2 J. G. Yu, L. J. Zhang, B. Cheng and Y. R. Su, Hydrothermal preparation and photocatalytic activity of hierarchically sponge-like macro-mesoporous titania, *J. Phys. Chem. C*, 2007, **111**, 10582–10586.

3 W. Zhou, F. F. Sun, K. Pan, G. H. Tian, B. J. Jiang, Z. Y. Ren, C. G. Tian and H. G. Fu, Well-ordered large-pore mesoporous anatase TiO$_2$ with remarkably high thermal stability and improved crystallinity: preparation, characterization, and photocatalytic performance, *Adv. Funct. Mater.*, 2011, **21**, 1922–1930.

4 G. Li, C. Liu and Y. Liu, Different effects of cerium ions doping on properties of anatase and rutile TiO$_2$, *Appl. Surf. Sci.*, 2006, **253**, 2481–2486.

5 A. Kumar and A. K. Jain, Photophysics and photochemistry of colloidal CdS–TiO$_2$ coupled semiconductors – photocatalytic oxidation of indole, *J. Mol. Catal. A: Chem.*, 2001, **165**, 265–273.

6 X. H. Xia, Z. J. Jia, Y. Yu, Y. Liang, Z. Wang and L. L. Ma, Preparation of multi-walled carbon nanotube supported TiO$_2$ and its photocatalytic activity in the reduction of CO$_2$ with H$_2$O, *Carbon*, 2007, **45**, 717–721.

7 V. M. Daskalaki, P. Panagiotopoulou and D. I. Kondarides, Production of peroxide species in Pt/TiO$_2$ suspensions under conditions of photocatalytic water splitting and glycerol photoreforming, *Chem. Eng. J.*, 2011, **170**, 433–439.

8 T. Sun, E. Z. Liu, J. Fan, X. Y. Hu, F. Wu, W. Q. Hou, Y. H. Yang and L. M. Kang, High photocatalytic activity of hydrogen production from water over Fe doped and Ag

deposited anatase TiO₂ catalyst synthesized by solvothermal method, *Chem. Eng. J.*, 2013, **228**, 896–906.

9 A. Ramchiary and S. K. Samdarshi, Ag deposited mixed phase titania visible light photocatalyst–Superiority of Ag-titania and mixed phase titania co-junction, *Appl. Surf. Sci.*, 2014, **305**, 33–39.

10 O. Rosseler, M. V. Shankar, M. K. L. Du, L. Schmidlin, N. Keller and V. Keller, Solar light photocatalytic hydrogen production from water over Pt and Au/TiO₂ (anatase/rutile) photocatalysts: Influence of noble metal and porogen promotion, *J. Catal.*, 2010, **269**, 179–190.

11 Y. Z. Yang, C. H. Chang and H. Idriss, Photocatalytic production of hydrogen form ethanol over M/TiO₂ catalysts (M = Pd, Pt or Rh), *Appl. Catal., B*, 2006, **67**, 217–222.

12 W. G. Wang, J. G. Yu, Q. J. Xiang and B. Cheng, Enhanced photocatalytic activity of hierarchical macro/mesoporous TiO₂–graphene composites for photodegradation of acetone in air, *Appl. Catal., B*, 2012, **119–120**, 109–116.

13 G. D. Jiang, Z. F. Lin, C. Chen, L. H. Zhu, Q. Chang, N. Wang, W. Wei and H. Q. Tang, TiO₂ nanoparticles assembled on graphene oxide nanosheets with high photocatalytic activity for removal of pollutants, *Carbon*, 2011, **49**, 2693–2701.

14 N. Raghavan, S. Thangavel and G. Venugopal, Enhanced photocatalytic degradation of methylene blue by reduced graphene-oxide/titanium dioxide/zincoxide ternary nanocomposites, *Mater. Sci. Semicond. Process.*, 2015, **30**, 321–329.

15 A. K. Geim and K. S. Novoselov, The rise of graphene, *Nat. Mater.*, 2007, **6**, 183–193.

16 K. I. Bolotin, K. J. Sikes, Z. Jiang, M. Klima, G. Fudenberg, J. Hone, P. Kim and H. L. Stormer, Ultrahigh electron mobility in suspended graphene, *Solid State Commun.*, 2008, **146**, 351–355.

17 D. C. Marcano, D. V. Kosynkin, J. M. Berlin, A. Sinitskii, Z. Z. Sun, A. Slesarev, L. B. Alemany, W. Lu and J. M. Tour, Improved synthesis of graphene oxide, *ACS Nano*, 2010, **4**, 4806–4814.

18 M. Shi, J. F. Shen, H. W. Ma, Z. Q. Li, X. Lu, N. Li and M. X. Ye, Preparation of graphene–TiO₂ composite by hydrothermal method from peroxotitanium acid and its photocatalytic properties, *Colloids Surf., A*, 2012, **405**, 30–37.

19 Y. J. Wang, R. Shi and T. Cordero, Significant photocatalytic enhancement in methylene blue degradation of TiO₂ photocatalysts *via* graphene-like carbon *in situ* hybridization, *Appl. Catal., B*, 2010, **100**, 179–183.

20 N. Prabhakarrao, M. Ravi Chandra and T. Siva Rao, Synthesis of Zr doped TiO₂/reduced Graphene Oxide (rGO) nanocomposite material for efficient photocatalytic degradation of Eosin Blue dye under visible light irradiation, *J. Alloys Compd.*, 2017, **694**, 596–606.

21 P. Nuengmatcha, S. Chanthai, R. Mahachai and W. Oh, Sonocatalytic performance of ZnO/graphene/TiO₂ nanocomposite for degradation of dye pollutants (methylene blue, texbrite BAC-L, texbrite BBU-L and texbrite NFW-L) under ultrasonic irradiation, *Dyes Pigm.*, 2016, **134**, 487–497.

22 Y. J. Li, X. M. Zhou, W. Chen, L. Y. Li, M. X. Zen, S. D. Qin and S. G. Sun, Photodecolorization of Rhodamine B on tungsten-doped TiO₂/activated carbon under visible-light irradiation, *J. Hazard. Mater.*, 2012, **227–228**, 25–33.

23 Z. Jafari, N. Mokhtarian, G. Hosseinzadeh, M. Farhadian, A. Faghihi and F. Shojaie, Ag/TiO₂/freeze-dried graphene nanocomposite as a high performance photocatalyst under visible light irradiation, *J. Energy Chem.*, 2016, **25**, 393–402.

24 N. R. Khalid, E. Ahmed, M. Ahmad, N. A. Niaz, M. Ramzan, M. Shakil, T. Iqbal and A. Majid, Microwave-assisted synthesis of Ag–TiO₂/graphene composite for hydrogen production under visible light irradiation, *Ceram. Int.*, 2016, **42**, 18257–18263.

25 Y. J. Li, S. Y. Zhang, Q. M. Yu and W. B. Yin, The effects of activated carbon supports on the structure and properties of TiO₂ nanoparticles prepared by a sol–gel method, *Appl. Surf. Sci.*, 2007, **253**, 9254–9258.

26 F. A. Jumeri, H. N. Lim, Z. Zainal, N. M. Huang and A. Pandikumar, Titanium dioxide-reduced graphene oxide thin film for photoelectrochemical water splitting, *Ceram. Int.*, 2014, **40**, 15159–15165.

27 M. N. Rashed and A. A. El-Amin, Photocatalytic degradation of methyl orange in aqueous TiO₂ under different solar irradiation sources, *Int. J. Phys. Sci.*, 2007, **2**, 73–81.

28 S. Qian, X. Y. Liu and C. X. Ding, Effect of Si-incorporation on hydrophilicity and bioactivity of titania film, *Surf. Coat. Technol.*, 2013, **229**, 156–161.

29 T. D. Nguyen-Phan, V. H. Pham, E. W. Shin, H. D. Pham, S. Kim, J. S. Chung, E. J. Kim and S. H. Hur, The role of graphene oxide content on the adsorption-enhanced photocatalysis of titanium dioxide/graphene oxide composites, *Chem. Eng. J.*, 2011, **170**, 226–232.

30 Y. Wang, Y. Huang, W. Ho, L. Zhang, Z. Zou and S. Lee, Biomolecule-controlled hydrothermal synthesis of C–N–S–tridoped TiO₂ nanocrystalline photocatalysts for NO removal under simulated solar light irradiation, *J. Hazard. Mater.*, 2009, **169**, 77–87.

31 X. Fan, J. Fan, X. Y. Hu, E. Z. Liu, L. M. Kang, C. N. Tang, Y. N. Ma, H. T. Wu and Y. Y. Li, Preparation and characterization of Ag deposited and Fe doped TiO₂ nanotube arrays for photocatalytic hydrogen production by water splitting, *Ceram. Int.*, 2014, **40**, 15907–15917.

32 B. Xin, L. Jing, Z. Ren, B. Wang and H. Fu, Effects of simultaneously doped and deposited Ag on the photocatalytic activity and surface states of TiO₂, *J. Phys. Chem. B*, 2005, **109**(7), 2805.

33 S. I. Mogal, V. G. Gandhi, M. Mishra, S. Tripathi, T. Shripathi, P. A. Joshi and D. O. Shah, Single-step synthesis of silver-doped titanium dioxide: influence of silver on structural, textural, and photocatalytic properties, *Ind. Eng. Chem. Res.*, 2014, **53**(14), 5749–5758.

34 N. D. Abazovic, L. Mirenghi, I. A. Jankovic, N. Bibic, D. V. Sojic, B. F. Abramovic and M. I. Comor, Synthesis and characterization of rutile TiO₂ nanopowders doped with iron ions, *Nanoscale Res. Lett.*, 2009, **4**, 518–525.

35 P. Wang, J. Wang, T. S. Ming, X. F. Wang, H. G. Yu, J. G. Yu, Y. G. Wang and M. Lei, Dye-Sensitization-Induced Visible-

Light Reduction of Graphene Oxide for the Enhanced TiO_2 Photocatalytic Performance, *ACS Appl. Mater. Interfaces*, 2013, **5**, 2924–2929.

36 J. Zhu, F. Chen, J. Zhang, H. Chen and M. Anpo, Fe^{3+}–TiO_2 photocatalysts prepared by combining sol–gel method with hydrothermal treatment and their characterization, *J. Photochem. Photobiol., A*, 2006, **180**, 196–204.

37 S. T. Nishanthi, S. Iyyapushpam, B. Sundarakannan, E. Subramanian and D. Pathinettam Padiyan, Plasmonic silver nanoparticles loaded titania nanotube arrays exhibiting enhanced photoelectrochemical and photocatalytic activities, *J. Power Sources*, 2015, **274**, 885–893.

38 M. Selim, A. S. Shah, K. Zhang, A. Reum Park, K. S. Kim, N. G. Park, J. H. Park and P. J. Yoo, Single-step solvothermal synthesis of mesoporous Ag–TiO_2–reduced graphene oxide ternary composites with enhanced photocatalytic activity, *Nanoscale*, 2013, **5**, 5093–5101.

39 P. Ciambelli, D. Sannino, V. Palma, V. Vaiano, R. S. Mazzei, P. Eloy and E. M. Gaigneaux, Photocatalytic cyclohexane oxidehydrogenation on sulphated MoO_x/γ-Al_2O_3 catalysts, *Catal. Today*, 2009, **141**(3–4), 367–373.

40 K. Eufinger, D. Poelman, H. Poelman, R. De Gryse and G. B. Marin, Effect of microstructure and crystallinity on the photocatalytic activity of TiO_2 thin films deposited by dc magnetron sputtering, *J. Phys. D: Appl. Phys.*, 2007, **40**, 5232–5238.